Progress in Natural Science: Materials International 2013;23(3):235–244

Chinese Materials Research Society

Progress in Natural Science: Materials International

www.elsevier.com/locate/pnsmi
www.sciencedirect.com

REVIEW

Nanostructured TiO_2(B): the effect of size and shape on anode properties for Li-ion batteries

Zheng Liu[a], Yuri G. Andreev[a], A. Robert Armstrong[a], Sergio Brutti[b], Yu Ren[c,*], Peter G. Bruce[a,]**

[a]*School of Chemistry and EaStChem, University of St Andrews, St Andrews, Fife KY16 9ST, UK*
[b]*Dipartimento di Scienze, Unversità della Basilicata, V.le Ateneo Lucano 10, Potenza 85100, Italy*
[c]*National Institute of Clean-and-low-carbon Energy (NICE), Future Science& Technology City, Changping, Beijing, 102209, China*

Received 26 September 2012; accepted 20 March 2013
Available online 18 June 2013

KEYWORDS

TiO_2(B);
Synthesis;
Anode;
Nanostructure;
Li-ion batteries

Abstract Reducing the dimensions of electrode materials from the micron to the nanoscale can have a profound influence on their properties and hence on the performance of electrochemical devices, e.g. Li-ion batteries, that employ such electrodes. TiO_2(B) has received growing interest as a possible anode for Li-ion batteries in recent years. It offers the possibility of higher energy storage compared with the commercialized $Li_4Ti_5O_{12}$. Bulk, nanowire, nanotube, and nanoparticle morphologies have been prepared and studied. However, to date these materials have not be compared in one article. In the current review we first summarize the different synthesis methods for the preparation of nanostructured TiO_2(B); then present the effects of size and shape on the electrochemical properties. Finally TiO_2(B) with nanometer dimensions exhibit a higher capacity to store Li, regardless of rate, due to structural distortions inherent at the nanoscale.

1. Introduction

TiO_2(B), although less well known than rutile, anatase, or brookite, is a better host for lithium intercalation than the other three (Fig. 1). "B" stands for bronze, by analogy with the tungsten bronze compounds. These four phases plus the other known TiO_2 polymorphs are listed in Table 1.

Titanates are being intensively investigated as anode materials for lithium-ion batteries due to their superior safety compared with graphite, Si, Sn or other low voltage anodes. Such safety arises in

*Corresponding author. Tel.: +86 10 57339664; fax: +86 10 57339649x9664.
**Corresponding author. Tel.: +44 1334 46 3825; fax: +44 1334 46 3808.
E-mail addresses: renyu@nicenergy.com (Y. Ren), p.g.bruce@st-andrews.ac.uk (P.G. Bruce).

Peer review under responsibility of Chinese Materials Research Society.

ELSEVIER Production and hosting by Elsevier

1002-0071 © 2013 Chinese Materials Research Society. Production and hosting by Elsevier B.V. All rights reserved.
http://dx.doi.org/10.1016/j.pnsc.2013.05.001

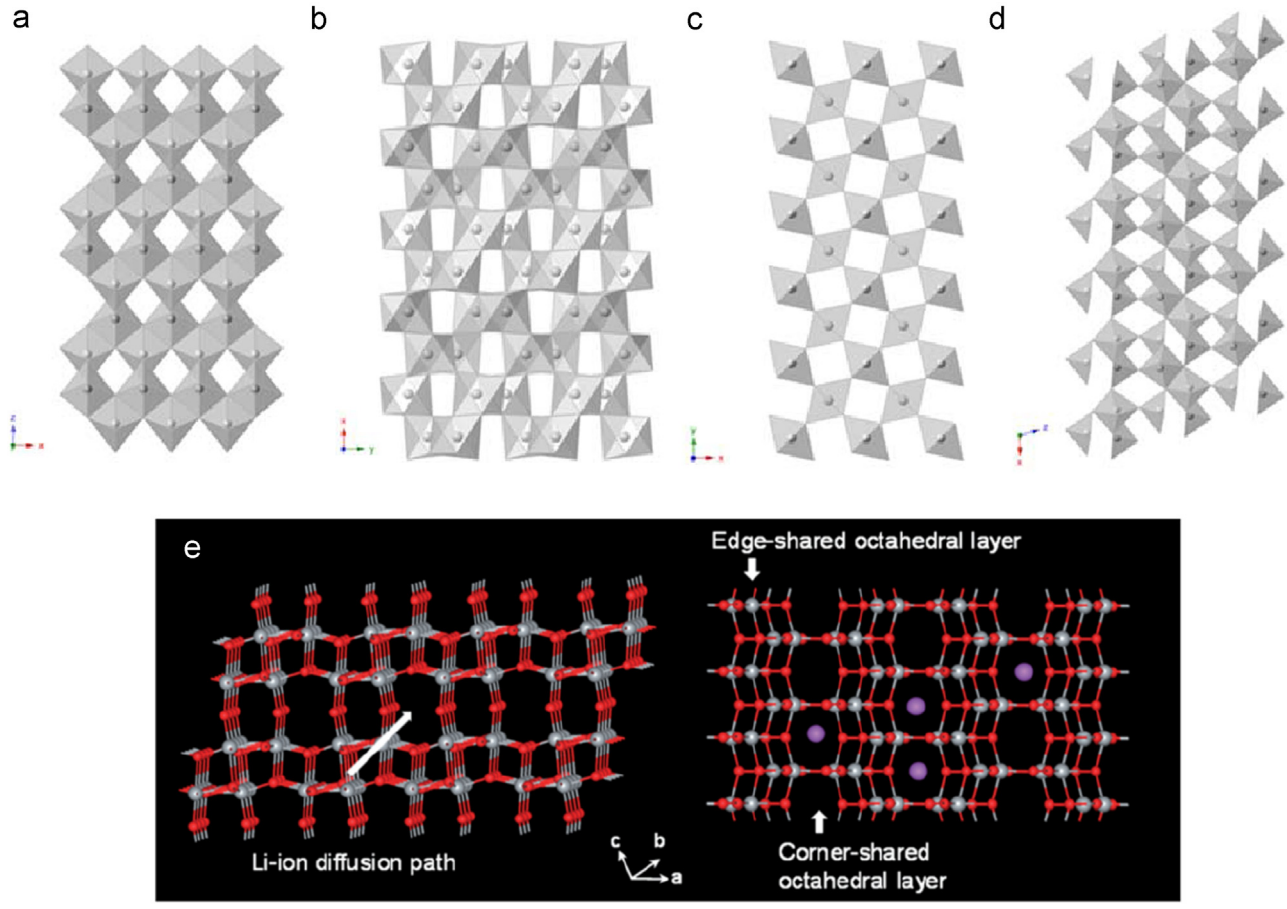

Fig. 1 The structure of (a) anatase, (b) brookite, (c) rutile, and (d) TiO_2(B); (e) the images of the TiO_2(B) structure before and after Li-intercalation, showing the preferred Li^+ diffusion path [12]. Reproduced with permission of the Royal Society of Chemistry from Ref. [12].

part from the high voltage of the titanates (1.5–1.7 V) compared with ~0 V for graphite, although, unless the high voltage anode is compensated by a high voltage cathode, the overall cell voltage will be reduced. One advantage of anodes operating at higher potential than graphite is that the cells can be charged at high rates with good safety. In order to achieve this high rate performance in the titanates it requires the use of nanostructured materials. Therefore much of the focus on titanate anodes has been on nanomaterials [1–13]. $Li_4Ti_5O_{12}$ spinel is now used as the anode in commercial lithium-ion batteries [14–17]. TiO_2 possesses twice the theoretical specific capacity (335 mAh/g) compared with $Li_4Ti_5O_{12}$ (175 mAh/g), i.e., has a specific capacity comparable to that of graphite, and as oxides have twice the density of graphite, they have twice the theoretical volumetric energy density (although nanostructuring can compromise this to an extent). These potential advantages render TiO_2 attractive as an anode for Li-ion batteries [2–8,10,12,13,18,19].

Some of the earliest work on titanate nanotubes/nanowires claimed the synthesis of TiO_2-anatase [20,21]. However, subsequent studies showed that the nanotubes/nanowires were composed of the layered titanate $H_2Ti_3O_7$ and the "scroll" mechanism of tube formation was proposed [22].

The titanate nanotubes/nanowires were generally prepared by the hydrothermal reaction between NaOH and anatase. We found that the composition and structure of both the tubes and wires are more complex than had been recognized previously [23,24]. The as-synthesized nanotubes and nanowires are sodium hydrogen titanates of general formula $Na_yH_{2-y}TinO_{2n+1} \cdot xH_2O$.Acid washing of such materials results in ion exchange to produce the layered hydrogen titanates $H_2Ti_nO_{2n+1} \cdot xH_2O$, which exhibit features similar to $H_2Ti_3O_7$, $H_2Ti_4O_9 \cdot H_2O$, and other members of the hydrogen titanate family. After controlled thermal treatment, the nanotubes transform into TiO_2(B) nanotubes [25].

In the following sections we will describe the synthesis of TiO_2(B) nanotubes, nanowires and the smallest nanoparticles of any titanate, their morpohology, mitigation of the first cycle irreversible capacity (a major problem and common feature of many nanostrucured electrodes), and the remarkable ability of nanostrucurred matetials to accommodate more Li than their bulk conternparts, regardless of rate.

2. Synthesis of different TiO_2(B) morphologies

2.1. *Bulk TiO_2(B)*

Bulk TiO_2(B) was first prepared by Marchand et al. in 1980 [29]. Synthesis involves high temperature solid state reaction between K_2CO_3 and TiO_2 to form $K_2Ti_4O_9$, ion exchange of K^+ with H^+ to form a hydrated hydrogen titanate, heating to 500 °C, thus inducing transformation into TiO_2(B). The resulting morphology

Table 1 Structure information of TiO_2 polymorphs.

Crystal form	Space group	Density	Synthesis method	Lithiation amout at bulk	Lithiation amout at nano
Anatase[26–28]	Tetragonal, I41/amd	3.79	–	0.5	1.0
Rutile[26–28]	Tetragonal, P42/mnm	4.13	–	0.1	0.85
Brookite[26,28]	Orthorhombic, Pbca	3.99	–	–	1.0
TiO_2(B), bronze[26,28,29]	Monoclinic, C2/m	3.64	Hydrolysis of $K_2Ti_4O_9$ followed by heating	0.71	1.0
TiO_2(H), hollandite-like form [26,28,30]	Tetragonal, I4/m	3.46	Oxidation of the related potassium titanate bronze, $K_{0.25}TiO_2$	–	–
TiO_2(R), ramsdellite-like form[28,31]	Orthorhombic, Pbnm	3.87	Oxidation of the related lithium titanate bronze $Li_{0.5}TiO_2$	–	–
TiO_2(II)-(α-PbO_2-like form) [26,28,32]	Orthorhombic, Pbcn	4.33	High pressure	–	–
TiO_2(III) (baddeleyite-like form, 7 coordinated Ti) [28,33]	Monoclinic	–	High pressure	–	–
TiO_2-OI [34]	Orthorhombic	–	High pressure	–	–
Cubic	Cubic	–	$P > 40$ GPa, $T > 1600$ °C	–	–
TiO_2 –OII ($PbCl_2$-like, 9 coordinated Ti) [35]	Orthorhombic	–	$P > 40$ GPa, $T > 700$ °C	–	–

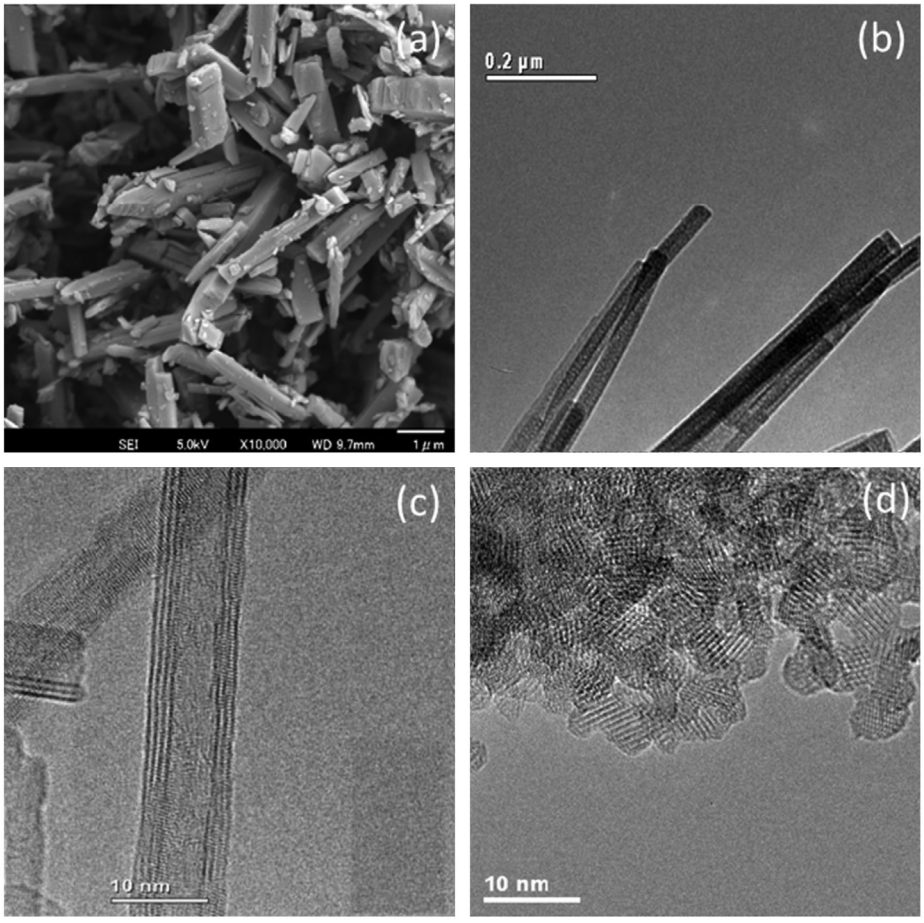

Fig. 2 SEM image of bulk TiO_2(B) (a) [36], TEM image of TiO_2(B) nanowires (b) [23], nanotubes (c) [24], and nanoparticles (d) [37]. Reproduced with permission of Elsevier from Ref. [36] (a), Wiley from Ref. [23] (b) and [37] (d), Royal Society of Chemistry from Ref. [24] (c).

is shown in Fig. 2a. The crystal are needle like and elongated along the *b* axis. They are typically several microns long and 0.2–0.8 μm wide.

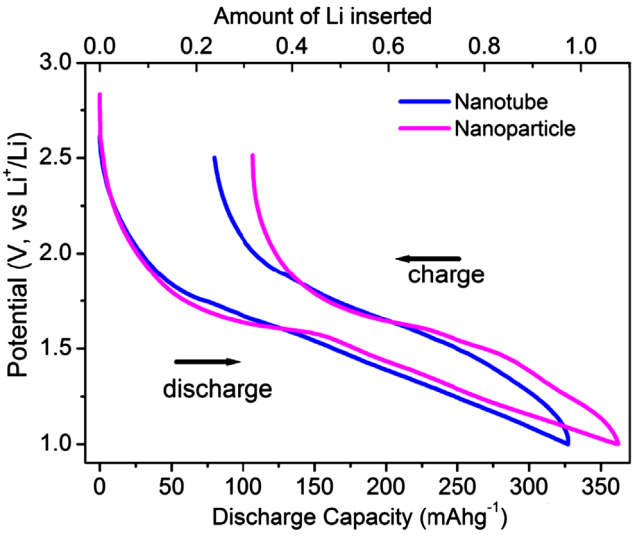

Fig. 3 The first cycle load curves of nanoparticle and nanotube TiO_2(B) at 10 mA/g.

2.2. *Nanowire*

Armstrong et al. first prepared TiO_2(B) nanowires [23,38]. The synthesis involved first adding the anatase TiO_2 into a 15 mol/L NaOH solution and hydrothermal treatment at 170 °C for 72 h. Then the product was acid wash with 0.05 mol/L HCl solution and finally calcined at 400 °C for 4 h in air. The nanowires are typically 20–40 nm in diameter and up to several microns long.

2.3. *Nanotube [24,39]*

The synthesis conditions for TiO_2(B) nanotubes are similar to those used for TiO_2(B) nanowire. TiO_2(B) nanotubes were synthesized by adding anatase into a solution of 15 mol/L NaOH followed by hydrothermal treatment at 150 °C for 72 h. Then the product of the hydrothermal reaction was washed with 0.05 mol/L of HCl, dried in air then heated to 400 °C for 5 h. The synthesis difference between the nanowires and nanotubes are the hydrothermal temperature and $NaOH/TiO_2$ ratio. The nanotubes are composed of walls of 2.5 nm thickness, with outer tube diameter 10 nm and up to several microns long.

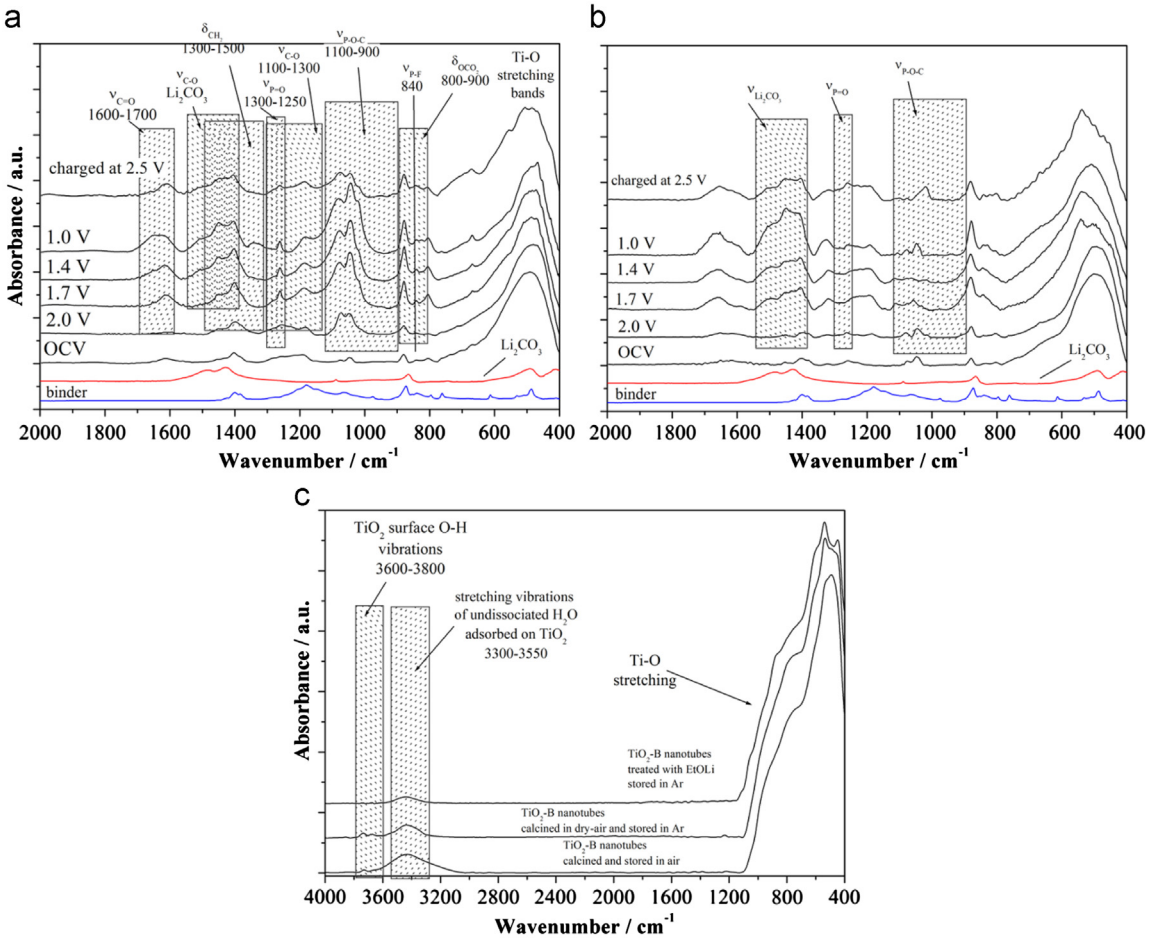

Fig. 4 (a) and (b) FTIR spectra collected on the TiO_2(B) electrodes at various states of discharge then charge. (c) FTIR of the different TiO_2(B) nanotubes with or without surface treatment. Dashed rectangles highlight the spectral regions within which particular functional group vibrations are observed [49]. Reproduced with permission of Wiley from Ref. [49].

2.4. *Nanoparticles[37]*

TiO_2(B) nanoparticles were prepared using a hydrothermal method modified from a previously reported procedure [40]. Metallic Ti was dissolved in a mixed solution of H_2O_2 and $NH_3 \cdot H_2O$ solution under ice/water bath; after addition of glycolate acid and adjustment of pH value by concentrated H_2SO_4, the solution was hydrothermally treated at 160 °C for 30 min. Finally, the solid was recovered at 60 °C over night and calcined at 300 °C for 1 h in dry air with a ramping rate of 1 °C/min. The obtained nanoparticles are all agglomerates, with primary particle size of 2.5×4.3 nm (from HRTEM analysis on 100 particles), and secondary particle size of 0.3–3 μm. Approximately half the primary particle surface area is in contact with other particles, based on BET surface area measurements [37].

3. Origin and mitigation of irreversible capacity

Although nanomaterials are receiving more and more interest as electrode materials for lithium-ion batteries, they generally suffer from large irreversible capacity loss on the first cycle (Fig. 3). This is a major issue that also affects nanosized titanates anode materials [41,42]. Such loss of capacity for intercalation electrodes in general has been attributed to the non-reversible Li intercalation on the first cycle [8,43–46] or the reaction between the electrolyte and the titanate surface [47,48]. The latter is believed more important for the nanosized titanate.

Using X-ray photoelectron spectroscopy (XPS) to follow the bulk composition and Fourier transform infra-red spectroscopy (FTIR) to follow the surface, during the first cycle, it has been shown that the irreversible capacity of TiO_2(B) nanotubes is indeed associated with the formation of a surface layer (Solid Electrolyte Interface) due to reaction between the TiO_2(B) surface and the electrolyte, Fig. 4.[49] The FTIR data collected from nanotubes on the first discharge (intercalation) and charge (deintercalation) shows that peaks grow that could be associated with Li_2CO_3 and $ROCO_2Li$ originating from solvent decomposition, $(RO,F)_3P{=}O$ and Li_xPF_y from $LiPF_6$ hydrolysis, similar to the SEI layer product of on carbon, Li metal, $Li_4Ti_5O_{12}$, or an oxides anode via conversion reaction [48,50–52]. It has also supplied strong evidence of the reduction of electrolyte on TiO_2(B) nanotube above 1–1.5 V, even above 2 V. After charge to 3 V, the intensity of the peaks decreases but they do not totally disappear (Fig. 4b).

In order to mitigate the irreversible capacity loss in the first cycle various surface chemical treatments of the TiO_2(B) nanotubes were investigated: treatment with the butyllithium, the CH_3CH_2OLi treatment, both before electrode preparation, and nano Li powder incorporation in the electrode formulation (nanoparticles of Li metal supplied by FMC corporation).

Using *n*-butyllithium or nanoparticle lithium powder, the high Coulombic efficiency of 97% and 94% can be obtained for TiO_2(B) nanotube on first cycle (Table 2). However, the reversible capacity is also decreased to 212 and 205 mAh/g, for *n*-butyllithium and nanoparticle lithium treated TiO_2(B) nanotubes, respectively, because of the chemical intercalation of Li reducing the remaining capacity for electrochemical lithium insertion on discharge. So there is a compromise between the low first cycle irreversible capacity and high reversible capacity for TiO_2(B) nanotubes. Using the lithium ethoxide treatment, the first discharge capacity is 237 mAh/g with an acceptable Coulombic efficiency of 93% (Table 2).

Since the surface of TiO_2(B) is covered with adsorbed H_2O and Ti–OH group (Fig. 4c), the reaction of hydroxyl with lithium ethoxide result in the reaction as follows: $Ti{-}O{-}H{+}C_2H_5OLi{=}Ti{-}O{-}Li$

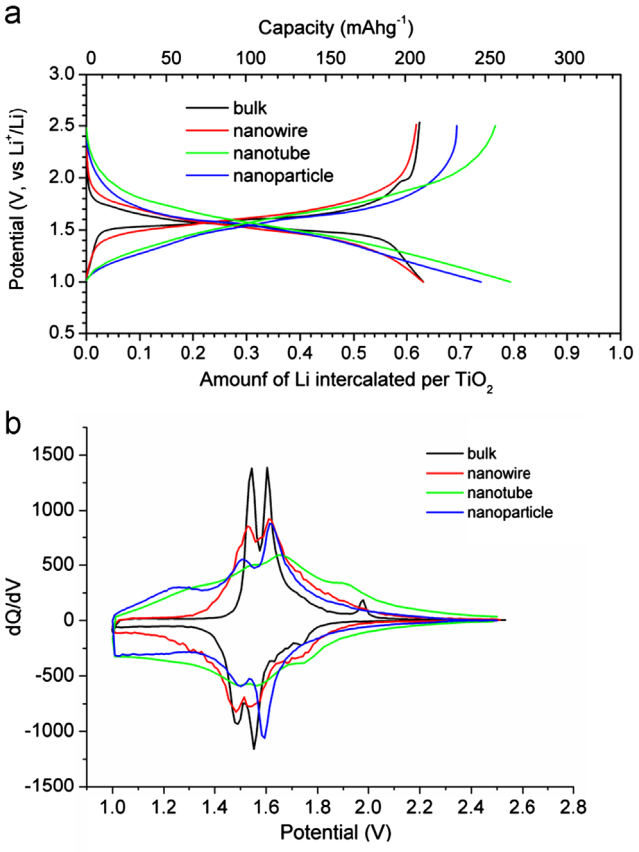

Fig. 5 Variation of voltage with state-of-charge for discharge then charge of bulk TiO_2(B), TiO_2(B) nanowires, nanotubes, and nanoparticles on the second cycle (a) and corresponding differential capacity plots (b). Rate 50 mAg^{-1}.

Table 2 Surface treatment effect on the electrochemistry of the TiO_2(B) nanotubes (i=C/20=17 mA/g).[49]. [49]. Reproduced with permission of Wiley from Ref. [49].

Structure	First discharge/charge capacity	First cycle coulombic efficiency (%)	Capacity retention at cycle 20 (%)
Nanotube	330/246	74	71
Nanotube+10 mol% BuLi	212/206	97	90
Nanotube+100 mol% CH_3CH_2OLi	237/220	93	90
Nanotube+20 mol% nanoLi	205/193	94	86

$+C_2H_5OH$, as derived from the decreased concentration of O–H group after surface treatment (Fig. 4c). This can help the mitigation of $LiPF_6$ hydrolysis, and the precipitation of LiF and organic phosphates. In summary, the surface treatments can greatly mitigate one of the major issues of nanosized electrode materials (e.g. titanates)-large first cycle irreversible capacity.

4. The influence of size on intercalation capacity

Once the surface layer has formed, the subsequent load curves correspond almost exclusively to lithium intercalation. As a result the comparison of electrochemical performance comparison among different nanostructured TiO_2(B) were carried on the second cycle at 50 mA/g.

The load curves on the second cycle and the corresponding differential capacity plots (d*Q*/d*V*) for all the TiO_2(B) materials are presented in Fig. 5. Some features of the electrochemistry for all four polymorphs are similar. All show a pair of plateaus in the load curves in the range 1.45–1.65 V. This is most clearly seen in the differential capacity plots (Fig. 5b), where peaks correspond to plateaus in the load curves. Such plateaus indicate to the presence of two 2-phase intercalation processes. In the cases of the bulk and nanowire TiO_2(B) materials, diffraction data of sufficient quality to apply established methods of structure elucidation (Rietveld refinement) can be obtained and have been used previously to assign the 2 phase processes to intercalation into the A1 and A2 sites of the TiO_2(B) crystal structure [53,54]. Intercalation into the same sets of sites may be occurring in the nanotubes and nanoparticles but here the diffraction peaks are too broad to be analyzed by Rietveld refinement, rendering it difficult to determine definitively the Li site occupancies by neutron diffraction. The peaks in the differential capacity plots broaden and lower in intensity as the dimensions of the TiO_2(B) particles are reduced, indicative of a transformation from 2-phase reactions, with constant chemical potential, towards a system that exhibits a Li chemical potential which varies with overall Li content. This is commensurate with previous observations of intercalation compounds that exhibit a two-phase intercalation process for large (bulk) particles but increasingly sloping load curves on reducing the particle dimensions [4,55–58].

Focusing on the effect of size on intercalation capacity, the dimensions of the nanoparticles (2.5 × 4.3 nm) and the wall thickness of the nanotubes (2.5 nm) are similar, whereas the nanowires (35 nm × 2 μm) are much closer to the dimensions of the bulk particles (200 nm × 2 μm). The nanoparticles and nanotubes can accommodate more Li and hence store more charge (~20–30%) than the bulk or nanowire morphologies (Fig. 5a). The additional capacity appears mainly below 1.4 V and may be seen in the difference between the areas under the differential capacity plots in Fig. 5b. The increased Li storage in ultrafine TiO_2(B) morphology (nanoparticle and nanotubes) compared with TiO_2(B) bulk and nanowires appears to be a general phenomenon due to the reduced dimensions. It is present at low rates and is not a kinetic phenomenon, the capacity increases on reducing the dimensions of crystalline materials to the nanoscale. In doing so, a greater proportion of the material will be in the near surface region where it is subjected to different forces than in the bulk, resulting in structural distortions. Such distortions have been

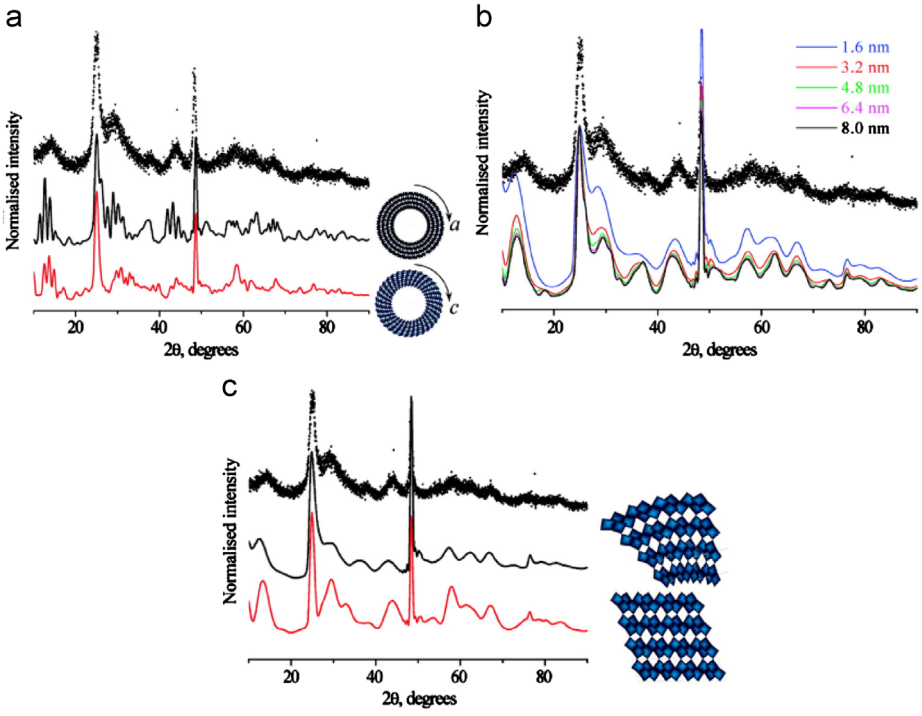

Fig. 6 (a) X-ray diffraction patterns of TiO_2(B) nanotubes: dots, observed pattern; black line, simulated pattern based on folding the *ab* plane of the ideal TiO_2(B) structure along *a* into a tube; red line, simulated pattern based on folding the *bc* plane of the ideal TiO_2(B) structure along *c* into a tube; (b) lines, simulated pattern based on folding the *ab* plane of the ideal TiO_2(B) structure along *a* into segments of the tube of different length around the circumference of the outer wall of the nanotube. Each segment consists of four layers in the radial direction.; (c) X-ray diffraction patterns of TiO_2(B) nanotubes: dots, observed pattern; black line, simulated pattern of a 3.2 nm tube segment corrected for preferred orientation; red line, simulated pattern of an ideal TiO_2(B) crystal structure (i.e., not distorted to form the tube) with the same number of atoms as the segment [25]. Reproduced with permission of the American Chemical Society from Ref. [25].

related to increased Li storage in TiO_2(B) nanotubes [25]. Establishing the structure (atomic arrangement) of nanomaterials is challenging because as the dimensions approach 1–2 nm long range translational symmetry is lost so is the ability to use crystallographic methods such as Rietveld refinement. An approach which provided the crucial structural data for TiO_2(B) nanotubes, without recourse the symmetry is described in the next section. Similar structural distortions are anticipated in the nanoparticles. A very small peak is evident at around 1.20–1.35 V on oxidation in the case of the nanotubes and nanoparticles that does not appear in the TiO_2(B) materials of larger dimension, understanding its origin also requires a detailed knowledge of the structural distortions.

5. Structure simulation of the TiO_2(B) nanotube [25]

The structures of nanosized TiO_2(B) can differ significantly from their bulk counterparts. However, determining the atomic structure of nanosized TiO_2(B) is difficult because the traditional crystallographic techniques rely on long-range ordered symmetry. For materials with particle sizes of only a few nanometers, their powder diffraction peaks become severely, and sometimes anisotropically, broadened, rendering the application of established crystallographic methods difficult or impossible.

Problems of structure elucidation apply to all nanomaterials, but the situation is particularly difficult for nanotubes of TiO_2(B). Not only their powder pattern is severely, and anisotropically, broadened due to the shape of nanometer dimensions (see Fig. 6), but, in addition, the ideal crystal structure is expected to distort as it curves to form the nanotube, introducing further violation of translational symmetry and, as a result, further peak broadening.

Use of the Debye equation, which requires no assumption of translational symmetry, permits not only to overcome the problems encountered by traditional powder diffraction techniques associated with anisotropic peak broadening but to use the latter in order to extract a more detailed structural information. Simply by applying this equation to a structural model of TiO_2(B) nanotubes, in the form of coordinates of all atoms within a tube, it is possible to simulate the complete powder diffraction profile and hence elucidate the deformed crystal structure.

A nanotube can be formed, for example, by folding the *ab* planes of the ideal TiO_2(B) structure along the *a* axis, with the *b* and *c* axes placed along the axial and radial directions of the tube, respectively (Fig. 6a).

A nanotube can be formed, for example, by folding the *ab* planes of the ideal TiO_2(B) structure along the *a* axis, with the *b* and *c* axes placed along the axial and radial directions of the tube, respectively (Fig. 6a).

Powders composed of particles with extreme aspect ratios often exhibit preferred orientation. Such an effect has been taken into account when calculating powder diffraction patterns from models of the TiO_2(B) nanotubes to further improve the fit to the experimental data. Various degrees of preferred orientation were examined, and the best description of the observed powder diffraction data was obtained for a preferred orientation parameter of 0.8 (see Fig. 6c). In excess of 90% of the TiO_2(B) powder is composed of nanotubes; however other morphologies may affect the diffraction profile, precluding refinement of the structure, hence, a precise representation of the observed powder pattern cannot be expected. Yet the simulation reproduces well the main features of the powder diffraction pattern, in particular the severe hkl-dependent broadening.

6. The rate capability of nanosized TiO_2(B)

Due to the poor electronic conductivity of the pure TiO_2(B) materials, large amount of carbon is generally needed to obtain good rate capability [38,39,59,60], which will reduce the volumetric energy density of TiO_2(B) materials. In the literatures, different components, e.g. metallic Au and Ag [61], Sn [62], carbon [63], graphene [64], CNT [65], even N etc., have been introduced into the TiO_2 to improve their conductivity

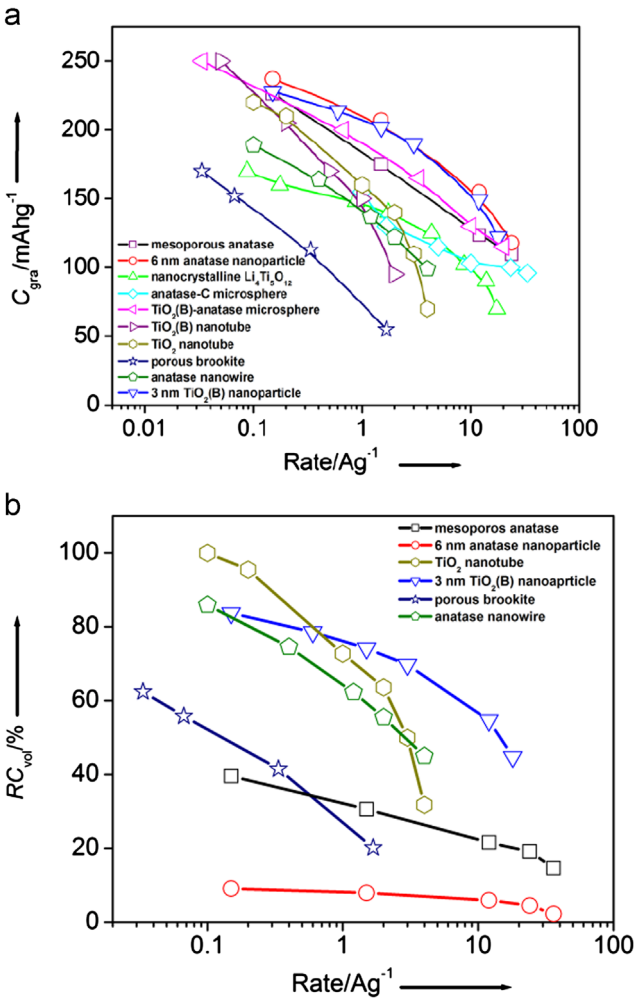

Fig. 7 (a) Gravimetric (C_{gra}) and (b) relative volumetric capacity (RC_{vol}) retention of TiO_2(B) nanoparticles compared with other titanate materials as a function of rate. The volumetric capacities are expressed relative to the highest value for the anatase nanotubes (synthesized from $H_2Ti_2O_5 \cdot H_2O$). For each electrode, the ratio of active material:carbon:binder and composite electrode density is given in brackets. Mesoporous anatase (black, 70:15:15) [43], 6 nm anatase nanoparticles (red, 50:45:5), nanocrystalline $Li_4Ti_5O_{12}$ (green, 85:15:5) [66], 94%anatase-6%C microspheres (cyan, 80:10:10) [67], 87%TiO_2(B)-13%anatase microspheres (mangenta, 70:15:15) [68], TiO_2(B) nanotubes (purple, 75:18:7) [39], TiO_2 nanotubes (anatase, from $H_2T_{i2}O_5 \cdot H_2O$, dark yellow, 75:15:10, 1.3 g/cm^3) [62], porous brookite (navy, 80:10:10 1.05 g/cm^3) [69], anatase nanowire (olive, 90:10:10, 1.3 g/cm^3) [70], and 3 nm TiO_2(B) nanoparticle (blue, 70:20:10, 1.05 g/cm^3). Only those materials for which electrode densities are available are presented in (b) Reproduced with permission of Wiley from Ref. [37].

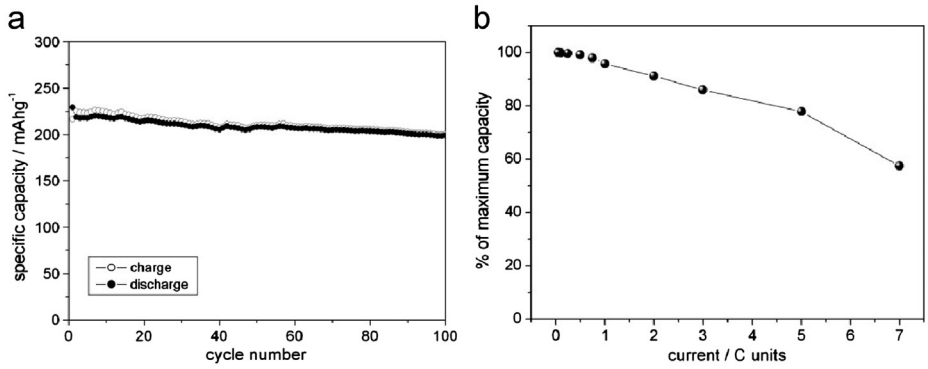

Fig. 8 (a) Variation of charge and discharge capacities versus cycle number for the TiO_2(B)–GPE–$LiNi_{0.5}Mn_{1.5}O_4$ battery cycled between 2 and 3.5 V at room temperature and at a rate of C/2; (b) Variation of discharge capacity as a function of rate, cycled between 2 and 3.5 V, expressed in terms of percentage of the maximum capacity obtained at low rate for the TiO_2(B)–GPE–$LiNi_{0.5}Mn_{1.5}O_4$ battery at room temperature [71]. Reproduced with permission of Wiley from Ref. [71].

and the rate capability. Due to the low thermal stability, the TiO_2(B) cannot be treated under temperature above 400 °C to obtain a highly conductive carbon coating as in the case of $LiFePO_4$. Interestingly, during tests on the electrochemical performance of nanoparticulate TiO_2(B), it is found that after mild thermal treatment of TiO_2(B) nanoparticles under dry air at 300 °C for 1 h, the material demonstrates extremely high power (rate capability), which is the best for all the reported titanate at rate > 1000 mA/g [37].

The variation of gravimetric capacity with different charge/discharge rates is shown in Fig. 7a, where the data of nanoparticulate TiO_2(B) are compared with several other titanate materials including nanoparticulate anatase (6 nm diameter), which corresponds to the best previously reported rate capability of any titanate [8,43]. The gravimetric capacity for the TiO_2(B) nanoparticles at all rates up to 18,000 mA/g is almost identical to the 6 nm anatase particles, which have a much higher proportion of carbon (45 wt%, significantly more than the TiO_2(B) nanoparticles and corresponding to a mass loading of only 1.5 mg/cm^2) in their composite electrodes.

The effect of diluting the active material by a large amount of carbon (as in the case of the 6 nm anatase nanoparticles) is evident on examining the volumetric capacity (based on the total volume of the composite electrode) as a function of rate (Fig. 7b). Nanoparticulate TiO_2(B) exhibits superior volumetric capacity at all rates compared with the 6 nm anatase material and the previously reported best high rate (> 1000 mA/g) volumetric capacity, namely mesoporous anatase. The relatively high volumetric capacity of the TiO_2(B) nanoparticles is in part due to the agglomerates formed by the primary nanoparticles, which helps to ensure a higher density of particles. The understanding of the cause of the high rate capability of TiO_2(B) nanoparticles will help the realization of high power of other TiO_2(B) anode materials in Li-ion batteries.

7. The incorporation of TiO_2(B) nanomaterials anodes into a full battery

Armstrong et al. incorporated the nanowire TiO_2(B) anode into a gel polymer electrolyte (GPE) based full battery [71]. Average cell potentials of approximately 2 and 3 V were obtained by using $LiFePO_4$ or $LiNi_{0.5}Mn_{1.5}O_4$ as the cathode, respectively. Cycling stability is very good as is rate capability, with 80% of the low-rate capacity being retained at 5C (Fig. 8). Anode-limited cells serve to demonstrate the superior capacity of these cells compared to similar batteries constructed using $Li_4Ti_5O_{12}$ instead of TiO_2(B) (225 mAh g^{-1} compared to 150 mAh g^{-1} at C/5). Combined with their superior safety and inherent overcharge protection compared to a graphite anode, and given the intense interest in developing lithium-ion cells with $Li_4Ti_5O_{12}$ anodes, the present results demonstrate the potential of TiO_2(B) as an anode in future lithium-ion batteries [71].

8. Conclusion

In this review, we have summarized the different synthesis methods for the nanostructured TiO_2(B); then we introduced the origin and mitigation of the first cycle irreversible capacity. The size effect on the electrochemistry properties, the nanostructure simulation and conductivity issues have also been discussed. The utilization of nanosized TiO_2(B) anode material in Li-ion batteries has to resolve the following hurdles: the irreversible capacity, the rate capability, and the volumetric energy density, which is of vital importance for the EV.

Acknowledgments

Y. Ren is indebted to Russell Trust for a travel grant. P.G. Bruce is grateful to the EPSRC including SUPERGEN and the program grant "Nanoionics" for financial support. Y. Ren is grateful to Shenhua Group for the funding support.

References

[1] K.M. Colbow, J.R. Dahn, R.R. Haering, Journal of Power Sources 26 (1989) 397.
[2] E. Ferg, R.J. Gummow, A. Dekock, M.M. Thackeray, Journal of the Electrochemical Society 141 (1994) L147.
[3] T. Ohzuku, A. Ueda, N. Yamamoto, Journal of the Electrochemical Society 142 (1995) 1431.
[4] G. Sudant, E. Baudrin, D. Larcher, J.M. Tarascon, Journal of Materials Chemistry 15 (2005) 1263.
[5] I. Plitz, A. DuPasquier, F. Badway, J. Gural, N. Pereira, A. Gmitter, G.G. Amatucci, Applied Physics A: Materials Science and Processing 82 (2006) 615.
[6] Y.G. Guo, Y.S. Hu, W. Sigle, J. Maier, Advanced Materials 19 (2007) 2087.

[7] M. Wagemaker, W.J.H. Borghols, F.M. Mulder, Journal of the American Chemical Society 129 (2007) 4323.
[8] C.H. Jiang, M.D. Wei, Z.M. Qi, T. Kudo, I. Honma, H.S. Zhou, Journal of Power Sources 166 (2007) 239.
[9] G.-N. Zhu, Y.-G. Wang, Y.-Y. Xia, Energy and Environmental Science 5 (2012) 6652.
[10] W.J.H. Borghols, M. Wagemaker, U. Lafont, E.M. Kelder, F.M. Mulder, Chemistry of Materials 20 (2008) 2949.
[11] M. Wagemaker, E.R.H. van Eck, A.P.M. Kentgens, F.M. Mulder, Journal of Physical Chemistry B 113 (2009) 224.
[12] D. Deng, M.G. Kim, J.Y. Lee, J. Cho, Energy and Environmental Science 2 (2009) 818.
[13] K. Amine, I. Belharouak, Z. Chen, T. Tran, H. Yumoto, N. Ota, S.-T. Myung, Y.-K. Sun, Advanced Materials 22 (2010) 3052.
[14] A. Du Pasquier, C.C. Huang, T. Spitler, Journal of Power Sources 186 (2009) 508.
[15] T. Tan, H. Yumoto, D. Buck, B. Fattig, C. Hartzog, World Electric Vehicle Journal 2 (2007) 76.
[16] N. Takami, K. Hoshina, H. Inagaki, Journal of the Electrochemical Society 158 (2011) A725.
[17] N. Takami, H. Inagaki, T. Kishi, Y. Harada, Y. Fujita, K. Hoshina, Journal of The Electrochemical Society 156 (2009) A128.
[18] P. Reale, S. Panero, B. Scrosati, Journal of The Electrochemical Society 152 (2005) A1949.
[19] L. Kavan, J. Prochazka, T.M. Spitler, M. Kalbac, M.T. Zukalova, T. Drezen, M. Gratzel, Journal of The Electrochemical Society 150 (2003) A1000.
[20] Y.X. Zhang, G.H. Li, Y.X. Jin, Y. Zhang, J. Zhang, L.D. Zhang, Chemical Physics Letters 365 (2002) 300.
[21] B.D. Yao, Y.F. Chan, X.Y. Zhang, W.F. Zhang, Z.Y. Yang, N. Wang, Applied Physics Letters 82 (2003) 281.
[22] Q. Chen, W.Z. Zhou, G.H. Du, L.M. Peng, Advanced Materials 14 (2002) 1208.
[23] A.R. Armstrong, G. Armstrong, J. Canales, P.G. Bruce, Angewandte Chemie International Edition 43 (2004) 2286.
[24] G. Armstrong, A.R. Armstrong, J. Canales, P.G. Bruce, Chemical Communications (2005) 2454.
[25] Y.G. Andreev, P.G. Bruce, Journal of the American Chemical Society 130 (2008) 9931.
[26] J.F. Banfield, D.R. Veblen, American Mineralogist 77 (1992) 545.
[27] D.T. Cromer, K. Herrington, Journal of the American Chemical Society 77 (1955) 4708.
[28] L. Kavan, M. Grätzel, S.E. Gilbert, C. Klemenz, H.J. Scheel, Journal of the American Chemical Society 118 (1996) 6716.
[29] R. Marchand, L. Brohan, M. Tournoux, Materials Research Bulletin 15 (1980) 1129.
[30] M. Latroche, L. Brohan, R. Marchand, M. Tournoux, Journal of Solid State Chemistry 81 (1989) 78.
[31] J. Akimoto, Y. Gotoh, Y. Oosawa, N. Nonose, T. Kumagai, K. Aoki, H. Takei, Journal of Solid State Chemistry 113 (1994) 27.
[32] P.Y. Simons, F. Dachille, Acta Crystallographica 23 (1967) 334.
[33] H. Sato, S. Endo, M. Sugiyama, T. Kikegawa, O. Shimomura, K. Kusaba, Science 251 (1991) 786.
[34] N.A. Dubrovinskaia, L.S. Dubrovinsky, R. Ahuja, V.B. Prokopenko, V. Dmitriev, H.P. Weber, J.M. Osorio-Guillen, B. Johansson, Physical Review Letters 87 (2001) 275501.
[35] L.S. Dubrovinsky, N.A. Dubrovinskaia, V. Swamy, J. Muscat, N.M. Harrison, R. Ahuja, B. Holm, B. Johansson, Nature 410 (2001) 653.
[36] M. Inaba, Y. Oba, F. Niina, Y. Murota, Y. Ogino, A. Tasaka, K. Hirota, Journal of Power Sources 189 (2009) 580.
[37] Y. Ren, Z. Liu, F. Pourpoint, A.R. Armstrong, C.P. Grey, P.G. Bruce, Angewandte Chemie International Edition 51 (2012) 2164.
[38] A.R. Armstrong, G. Armstrong, J. Canales, R. Garcia, P.G. Bruce, Advanced Materials 17 (2005) 862.
[39] G. Armstrong, A.R. Armstrong, J. Canales, P.G. Bruce, Electrochemical and Solid-State Letters 9 (2006) A139.
[40] M. Kobayashi, V.V. Petrykin, M. Kakihana, Chemistry of Materials 19 (2007) 5373.
[41] P.G. Bruce, B. Scrosati, J.M. Tarascon, Angewandte Chemie International Edition 47 (2008) 2930.
[42] A.S. Arico, P. Bruce, B. Scrosati, J.M. Tarascon, W. Van Schalkwijk, Nature Materials 4 (2005) 366.
[43] Y. Ren, L.J. Hardwick, P.G. Bruce, Angewandte Chemie International Edition 49 (2010) 2570.
[44] A.G. Dylla, G. Henkelman, K.J. Stevenson, Accounts of Chemical Research, Article ASAP http://dx.doi.org/10.1021/ar300176y.
[45] C.H. Jiang, I. Honma, T. Kudo, H.S. Zhou, Electrochemical and Solid-State Letters 10 (2007) A127.
[46] P. Poizot, S. Laruelle, S. Grugeon, L. Dupont, J.M. Tarascon, Nature 407 (2000) 496.
[47] D. Aurbach, B. Markovsky, I. Weissman, E. Levi, Y. Ein-Eli, Electrochimica Acta 45 (1999) 67.
[48] P. Verma, P. Maire, P. Novák, Electrochimica Acta 55 (2010) 6332.
[49] S. Brutti, V. Gentili, H. Menard, B. Scrosati, P.G. Bruce, Advanced Energy Materials 2 (2012) 322.
[50] G. Gachot, S. Grugeon, M. Armand, S. Pilard, P. Guenot, J.-M. Tarascon, S. Laruelle, Journal of Power Sources 178 (2008) 409.
[51] M.K. Rahman, Y. Saito, Journal of Power Sources 174 (2007) 889.
[52] H. Ota, A. Kominato, W.-J. Chun, E. Yasukawa, S. Kasuya, Journal of Power Sources 119–121 (2003) 393.
[53] A.R. Armstrong, C. Arrouvel, V. Gentili, S.C. Parker, M.S. Islam, P. G. Bruce, Chemistry of Materials 22 (2010) 6426.
[54] L. Brohan, R. Marchand, Solid State Ion 9–10 (1983) 419.
[55] P. Gibot, M. Casas-Cabanas, L. Laffont, S. Levasseur, P. Carlach, S. Hamelet, J.-M. Tarascon, C. Masquelier, Nature Materials 7 (2008) 741.
[56] N. Meethong, H.Y.S. Huang, W.C. Carter, Y.M. Chiang, Electrochemical and Solid-State Letters 10 (2007) A134.
[57] G. Kobayashi, S.-i. Nishimura, M.-S. Park, R. Kanno, M. Yashima, T. Ida, A. Yamada, Advanced Functional Materials 19 (2009) 395.
[58] L.J. Hardwick, M. Holzapfel, P. Novak, L. Dupont, E. Baudrin, Electrochimica Acta 52 (2007) 5357.
[59] T. Beuvier, M. Richard-Plouet, M. Mancini-Le Granvalet, T. Brousse, O. Crosnier, L. Brohan, Inorganic Chemistry 49 (2010) 8457.
[60] J. Li, W. Wan, H. Zhou, J. Li, D. Xu, Chemical Communications 47 (2011) 3439.
[61] S.H. Nam, H.-S. Shim, Y.-S. Kim, M.A. Dar, J.G. Kim, W.B. Kim, ACS Applied Materials and Interfaces 2 (2010) 2046.
[62] H. Kim, M.G. Kim, T.J. Shin, H.-J. Shin, J. Cho, Electrochemistry Communications 10 (2008) 1669.
[63] Z. Yang, G. Du, Z. Guo, X. Yu, Z. Chen, T. Guo, H. Liu, Journal of Materials Chemistry, 21, 8591.
[64] F. Wang, K. Zhang, Journal of Molecular Catalysis A: Chemical, 345, 101.
[65] Q. Wang, Z.H. Wen, J.H. Li, Advanced Functional Materials 16 (2006) 2141.
[66] A.S. Prakash, P. Manikandan, K. Ramesha, M. Sathiya, J.M. Tarascon, A.K. Shukla, Chemistry of Materials 22 (2010) 2857.
[67] F.-F. Cao, X.-L. Wu, S. Xin, Y.-G. Guo, L.-J. Wan, Journal of Physical Chemistry C 114 (2010) 10308.
[68] H. Liu, Z. Bi, X.-G. Sun, R.R. Unocic, M.P. Paranthaman, S. Dai, G.M. Brown, Advanced Materials 23 (2011) 3450.
[69] D. Dambournet, I. Belharouak, K. Amine, Chemistry of Materials 22 (2009) 1173.
[70] M.G. Kim, H. Kim, J. Cho, Journal of the Electrochemical Society 157 (2010) A802.
[71] G. Armstrong, A.R. Armstrong, P.G. Bruce, P. Reale, B. Scrosati, Advanced Materials 18 (2006) 2597.

Peter Bruce (FRS, FRSE, FRSC), is Wardlaw Professor of Chemistry at the University of St Andrews. His research interests embrace materials chemistry and electrochemistry, and include the synthesis and characterisation of new materials with new properties or combinations of properties for new generations of energy conversion and storage devices, especially lithium batteries. Recent work has focussed on nano-intercalation materials, new methods of structure determination and the potentially transformational Li-air battery. His research has been recognised by a number of awards and fellowships, including from the Royal Society, the Royal Society of Chemistry, The Electrochemical Society and the German Chemical Society.

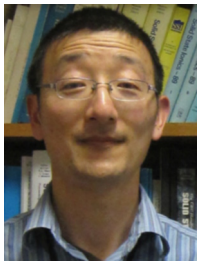

Yu Ren received M.Sc. (2003) from Fudan University in the field of porous silicates, adsorption, and catalysis with Prof. Heyong He. After 3 years in industry, he went to UK and worked on Li-ion batteries and nanoionics. He obtained Ph.D. degree (2010) under supervision of Prof. Peter Bruce and continued as a Postdoc thereafter. Since September 2011, Dr. Ren joined the National Institute of Clean-and-low-carbon Energy (NICE), Shenhua Group. Currently Dr. Ren has broad research interests in energy storage (Li-ion batteries, supercapacitors), materials chemistry, and heterogeneous catalysis.